

X-ray microdiffraction study of growth modes and crystallographic tilts in oxide films on metal substrates

JOHN D. BUDAI^{*1}, WENGE YANG¹, NOBUMICHI TAMURA², JIN-SEOK CHUNG³, JONATHAN Z. TISCHLER¹, BENNETT C. LARSON¹, GENE E. ICE⁴, CHAN PARK⁵ AND DAVID P. NORTON⁶

¹Condensed Matter Sciences Division, Oak Ridge National Laboratory, PO Box 2008, Oak Ridge, Tennessee 37831, USA

²Advanced Light Source, 1 Cyclotron Road, Lawrence Berkeley National Laboratory, Berkeley, California 94720, USA

³Department of Physics, Soongsil University, 1-1 Sangdo-dong, Seoul, South Korea

⁴Metals & Ceramics Division, Oak Ridge National Laboratory, PO Box 2008, Oak Ridge, Tennessee 37831, USA

⁵Korea Electrotechnology Research Institute, 28-1 Seong Joo Dong, Changwon, South Korea

⁶Department of Materials Science & Engineering, University of Florida, Gainesville, Florida 32611, USA

*e-mail: budaijd@ornl.gov

Published 8 June 2003; doi:10.1038/nmat916

The crystallographic texture of thin-film coatings plays an essential role in determining such diverse materials properties as wear resistance, recording density in magnetic media and electrical transport in superconductors. Typically, X-ray pole figures provide a macroscopically averaged description of texture, and electron backscattering provides spatially resolved surface measurements. In this study, we have used focused, polychromatic synchrotron X-ray microbeams to penetrate multilayer materials and simultaneously characterize the local structure, orientation and strain tensor of different heteroepitaxial layers with submicrometre resolution. Grain-by-grain microstructural studies of cerium oxide films grown on textured nickel foils reveal two distinct kinetic growth regimes on vicinal surfaces: ledge growth at elevated temperatures and island growth at lower temperatures. In addition, a combinatorial approach reveals that crystallographic tilting associated with these complex interfaces is qualitatively described by a simple geometrical model applicable to brittle films on ductile substrates. The sensitivity of conducting percolation paths to tilt-induced texture improvement is demonstrated.

After early studies of high-temperature superconducting materials such as YBaCuO revealed that high-angle grain boundaries act as severe weak links for current transport^{1,2}, substantial research has been directed towards the development of long lengths of crystallographically aligned superconductors³. One approach has been to induce alignment using the epitaxial growth of oxide films on rolling-assisted biaxially textured substrates (RABiTS)⁴. Rolled Ni substrates are recrystallized under conditions that lead to a high degree of biaxial {001} <100> cube texture. Subsequent growth of epitaxial oxide buffer layers (typically CeO₂ and YSZ as chemical barriers) and superconducting YBCO preserves the alignment, enabling high critical current densities, $J_c > 10^6$ cm⁻². Conventional monochromatic X-ray ω - and ϕ -scans typically reveal macroscopic biaxial texture to within $\sim 5^\circ$ – 10° full-width at half-maximum (FWHM) for all layers, but do not describe local microstructural features that control the materials properties. We note that in the case of brittle oxide films on ductile metal substrates, epitaxial growth involves strain interactions between two materials with disparate elastic properties. Understanding and controlling the local texture and microstructural evolution of processes associated with heteroepitaxial growth, differential thermal contraction and cracking remain significant challenges in this complex system^{5,6}, as well as in many other technologically important thin-film applications.

In this article, we report results using X-ray microdiffraction techniques^{7–11} to penetrate both the oxide layer and the substrate to investigate the epitaxial growth of cerium oxide (CeO₂) films on textured Ni substrates deposited by pulsed laser deposition (PLD). Figure 1a illustrates the microbeam diffraction geometry for a film on a textured polycrystalline substrate. The focused polychromatic synchrotron beam is diffracted from a submicrometre-diameter area within a single grain of the CeO₂/Ni sample, producing complete diffraction patterns (Fig. 1b) from each layer on the charge-coupled-device area detector. Quantitative analysis of the Laue patterns yields the local lattice orientation (resolution $\sim 0.01^\circ$) and deviatoric strain tensor (resolution $\sim 10^{-4}$) for each layer¹². The patterns show that the cubic fluorite CeO₂ and face-centred-cubic Ni principal in-plane

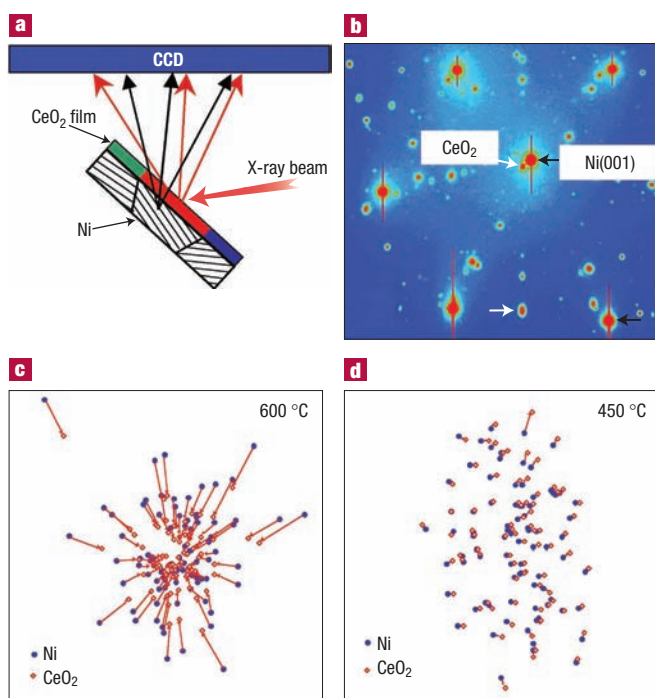


Figure 1 Grain-by-grain white-beam X-ray microdiffraction from a film deposited on a polycrystalline substrate. **a**, Focused synchrotron beam incident on the sample and diffracting into area charge-coupled-device (CCD) detector. **b**, CCD detector image showing simultaneous local Laue (001) patterns from both CeO₂ film and Ni substrate. **c**, Relative locations of local Ni(001) and CeO₂(001) poles on the detector for film grown at high temperature, 600 °C. **d**, Locations of Ni and CeO₂ poles for film grown at low temperature, 450 °C.

crystallographic axes are related by the expected 45° rotation, corresponding to ~9% lattice mismatch. However, Fig. 1b also shows that the out-of-plane film and substrate (001) plane normals are not exactly aligned. Instead, we observe a crystallographic tilt of the oxide lattice relative to the Ni lattice, typically with the film [001] pole tilting towards alignment with the sample surface normal. Note that microbeam patterns at different locations on a single sample provide measurements from a large number of grains with different vicinal surfaces grown under identical conditions. Previous investigations of epitaxy on off-axis surfaces required that a new sample be grown on a large single crystal for each miscut angle. Thus, observations were limited and susceptible to reproducibility errors. The X-ray microbeam and a textured substrate eliminate these limitations and, in effect, enable a combinatorial approach to the measurement of heteroepitaxial growth.

To investigate the heteroepitaxial tilting mechanism and its dependence on kinetics, a set of CeO₂ films on Ni substrates were grown at four different temperatures over the range 450–785 °C under otherwise identical PLD conditions¹³. Here, all CeO₂ films were 0.5 μm thick and were deposited in an initially reducing atmosphere (4% H₂/Ar, 0.1 torr) onto 50-μm-thick textured Ni (mosaic ~8° FWHM) foils. X-ray microdiffraction Laue patterns (0.7-μm-diameter beam) at many positions on each of the three higher-temperature samples (600, 700 and 785 °C) appeared very similar, exhibiting sharp Bragg peaks and significant tilting of the CeO₂ (001) pole towards the surface normal. The patterns from the lowest temperature deposition (450 °C) had a different appearance, exhibiting weak, diffuse CeO₂ peaks, which were more closely aligned with the substrate reflections. Thus, the

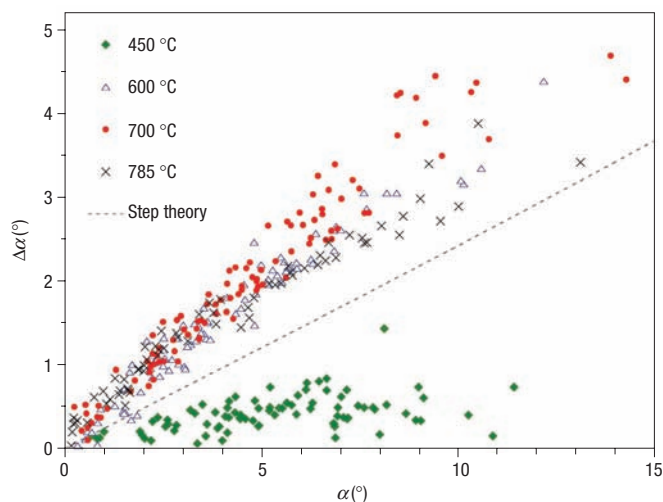


Figure 2 Crystallographic tilt, $\Delta\alpha$, of the CeO₂(001) planes relative to the substrate Ni(001) planes. Plots are as a function of the local Ni(001) miscut angle, α , for heteroepitaxial oxide films grown at four different substrate temperatures 450–785 °C. The dashed line indicates the result of a geometrical coherency model with no fitting parameters (see text).

lowest-temperature film has smaller coherently scattering domains and almost no tilts. These differing orientation tendencies are illustrated in Fig. 1c,d, where the location of the Ni(001) and CeO₂(001) poles on the detector are indicated for a large number of individual grains in samples grown at 600 °C and 450 °C. Note that the centre of the detector area corresponds to the sample normal in our diffraction geometry. At high temperatures, the film and substrate (001) poles clearly shift further apart as the substrate (001) orientation moves away from the normal (that is, the miscut angle increases). In contrast, the low-temperature CeO₂(001) poles exhibit only a small angular bias (~0.5°) predominantly in the same direction in Fig. 1d, that is, towards the right rather than towards the centre.

We have quantified the crystallographic observations by fitting peaks and indexing each Laue pattern (angular resolution ~0.01°) to obtain the local orientation matrix. The out-of-plane tilt angle, $\Delta\alpha$, between the CeO₂(001) and Ni(001) planes as a function of the local substrate surface miscut angle, α , is plotted in Fig. 2 for the four growth temperatures. The measurements show that the two angles are remarkably well correlated. At high growth temperatures, the relation is approximately linear with a slope of ~0.45–0.5, levelling somewhat at large miscut angles above 10°. At low temperatures, $\Delta\alpha$ is much smaller in magnitude and more scattered. The quantitative analysis reveals that there is no significant in-plane component to the crystallographic tilts; that is, the film <110> and substrate <100> axes are aligned in-plane. Further, we observe no dependence of the out-of-plane component (c axis) on the in-plane azimuthal direction of the miscut. Because the CeO₂[001] tilts are consistently towards the surface normal, the microbeam data explains why the macroscopic X-ray rocking curves for the oxide films in RABiTS samples generally are narrower than for the underlying Ni substrate^{4,13}. However, it more importantly shows that the angular differences between the film and substrate are not random spatially, but instead are intrinsically related by the local vicinal surface angle. Film tilts are not statistical; they are locally determined.

The systematic, linear dependence of crystallographic tilt on local miscut shown in Fig. 2 demonstrates that reproducible microstructural mechanisms control the epitaxial alignment during

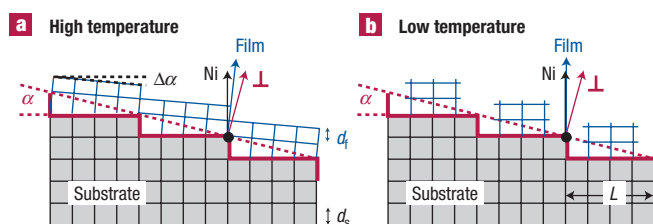


Figure 3 Heteroepitaxial growth modes for CeO₂ films on textured Ni substrates.

a, Growth proceeds by step-ledge propagation with crystallographic tilts at high substrate temperatures. α is the local substrate surface miscut angle; $\Delta\alpha$ is the out-of-plane tilt angle; d_s is the out-of-plane substrate lattice spacing, d_f is the relaxed film lattice spacing. **b**, Film deposition begins with island formation on flat terraces (of distance L) at low substrate temperatures.

high-temperature growth. Although crystallographic tilting of heteroepitaxial films is a general phenomenon observed in many materials, the microstructural origins remain poorly understood, especially for large-misfit systems^{14–23}. The most extensive analyses have been carried out on high-purity, single-crystal semiconductor systems owing to the importance of strain and defect effects on electronic properties. By comparison with semiconductor heterostructures, the CeO₂/Ni system has a high concentration of impurities (Ni ~99.99%), many extrinsic defects, large lattice mismatch (~9%), and disparate elastic (brittle on ductile) properties. Given the comparatively ‘dirty’ (that is, imperfect) nature of this system, we find it remarkable that well-defined tilts are in fact observed. As will be shown later, systematic tilts towards the surface normal give rise to enhanced texture in the film, an extremely useful result in many applications.

Two general types of microstructural mechanisms have classically been identified as responsible for orientation changes: step-mismatch mechanisms and biased dislocation mechanisms. Geometrical ‘intrinsic’ tilt mechanisms, first proposed by Nagai¹⁴, consider the effect of elastic strain due to lattice mismatch at surface steps on miscut surfaces during the initial stages of film deposition. As the film thickness increases beyond a critical value, misfit dislocations may be introduced for strain relaxation. At this point, the second type of crystallographic tilt mechanism is activated if particular types of dislocations with a net out-of-plane component to the Burger vectors are preferentially inserted. For miscut substrates, the direction of the ledges can provide the bias favouring the activation of particular dislocation systems.

The microdiffraction CeO₂/Ni measurements can be understood by assuming that the tilt mechanisms described above are kinetically inoperative at the lowest temperature (450 °C) and are activated at the higher growth temperatures (600–800 °C). The contrasting growth modes are illustrated schematically in Fig. 3. At 450 °C, surface mobility is suppressed so that isolated islands are nucleated initially on the flat terraces. Because nucleation and growth on the terraces do not involve the steps, the crystallographic orientation of the substrate should be preserved in the film. At the higher temperatures, the deposited material has sufficient surface mobility that growth proceeds by step-ledge propagation, activating the crystallographic tilt mechanisms. In this case, the substrate miscut angle plays a central role by defining the ledge density.

Examining the low-temperature growth in more detail, the proposed island model shown in Fig. 3b assumes that the surface steps have no effect on epitaxy, and hence predicts $\Delta\alpha \approx 0$ for all miscuts. However, the data does exhibit a small tilt bias of $\sim 0.5^\circ$ in a preferred direction. We believe that this weak tendency is due to slightly off-axis deposition of the energetic ions in the plume during PLD. The film

alignment with the incident beam direction has been attributed to ion channelling and damage effects, and is used at large inclinations to orient films during ion-beam-assisted deposition²⁴ and inclined substrate deposition²⁵. We further note that the observation of smaller, coherently scattering domains at low temperature is consistent with ion damage, low surface mobility, and a high density of island nucleation sites. Clearly, the high angular resolution ($\sim 0.01^\circ$) provided by X-ray microdiffraction will enable more systematic studies of the effect of intentionally off-axis depositions on the microstructure.

For analysing the high-temperature tilts in more detail, a general theory must consider both types of crystallographic tilting mechanisms introduced above. During the initial stages of film growth, the ‘intrinsic’ Nagai contribution corresponds to the situation where a thin CeO₂ (001) film is tetragonally strained to match the out-of-plane substrate lattice spacing, d_s , at the surface ledge, but is free to relax to the unstrained film value, d_f , across each terrace distance, L . The direction of the tilt misorientation of the film [001] from the Ni [001] is towards the surface normal for $d_f < d_s$ (as illustrated in Fig. 3a) and away from the normal for $d_f > d_s$. For a local substrate miscut angle, α , the step-matching requirement introduces a tilt between the film and the substrate, $\Delta\alpha$, given by^{14,17,20}

$$\Delta\alpha = \tan^{-1} \left(\frac{d_s - d_f}{d_s} \tan \alpha \right). \quad (1)$$

This expression is plotted as the dashed line in Fig. 2, using monolayer step heights $d_s = 1.78 \text{ \AA}$ for Ni and $d_f = 1.36 \text{ \AA}$ for CeO₂ at $\sim 700 \text{ }^\circ\text{C}$. The agreement between the measurements and the theory is only qualitative, with the theory underestimating the magnitude of the observed tilts.

It is possible that the second class of tilt mechanisms, the biased nucleation and motion of misfit dislocations, is responsible for additional crystallographic tilting. In contrast with systems with more homogeneous elastic properties, if dislocations are mobile here, the plastic deformation may occur predominantly in the compliant, ductile metal substrate rather than in the relatively stiff, brittle oxide film²⁶. Consequently, the film orientation may not be affected by dislocation kinetics. In Fig. 2, the three high-temperature samples show approximately the same slope, $\Delta\alpha/\alpha$, supporting the view that kinetically activated dislocation mechanisms do not significantly affect the crystallographic tilts. Alternative origins for additional tilting may involve surface segregation of impurity atoms²⁷ or non-stoichiometry of the initial CeO₂ layers. Either of these mechanisms can modify the effective ledge heights and hence quantitatively affect the tilts. In principle, transmission electron microscopy and other techniques could provide information elucidating the detailed roles of interfacial dislocations and impurities. Unfortunately, characterization studies are difficult due to large thermal contraction strains and the formation of a NiO layer during later stages of film growth, which obscure the microstructure present during initial stages of growth^{5,28}.

Crystallographic tilting associated with step-matching during ledge growth described above should apply broadly to stiff films on easily deformed substrates. Indeed, we have such evidence; initial microbeam measurements obtained from two other oxide films deposited at high temperatures on textured Ni(001) foils by PLD suggest that the intrinsic tilt mechanism is general. We find that yttria-stabilized zirconia (YSZ)²⁹ and LaMnO₃ (LMO)³⁰ films also exhibit clear crystallographic tilts between the film and substrate (001) poles. Although the reflections are more diffuse, the YSZ shifts are qualitatively similar to the CeO₂ results, with tilts consistently towards the surface normal. Like CeO₂, YSZ has a cubic fluorite structure with a monolayer d -spacing ($\sim 1.30 \text{ \AA}$ at 700 °C) smaller than the Ni spacing. In contrast, the LMO(001) poles shift in the opposite direction, away from the surface normal. LMO possesses a pseudo-cubic perovskite structure with monolayer spacing ($\sim 2.00 \text{ \AA}$ at 700 °C) larger than Ni. Thus, in both additional cases, the crystallographic tilts are in qualitative agreement with the prediction

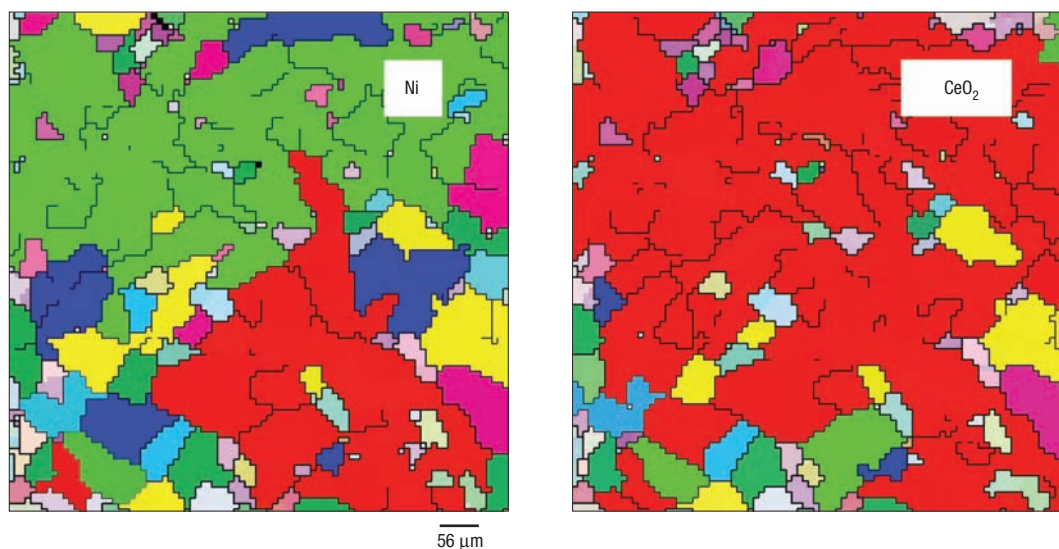


Figure 4 Orientation maps produced by X-ray microdiffraction. Black lines indicate boundaries between pixels where the total misorientation (including both in-plane and out-of-plane components) is greater than 5° . Each coloured area shows a percolative region connected by boundaries of less than 5° .

of the simple geometrical construction presented above. Taken together, the observations from the three oxide film systems provide compelling evidence that the simple intrinsic model discussed above qualitatively describes a dominant microstructural mechanism responsible for the crystallographic tilts. Additional studies examining atomic-level surface structure and dislocation kinetics during the initial stages of growth will be required to quantitatively establish the roles of all mechanisms, in particular epitaxial systems.

The crystallographic tilts revealed here are of significant practical importance, because the misorientation angles between neighbouring grains strongly impact the critical current transport in coated superconductor applications^{1,3}. Texture development in oxide superconductors has been studied extensively³¹, and the effect of alignment on percolation and transport has been modelled by several groups^{32–38}. Because the critical current density of a grain boundary decreases exponentially with the misorientation angle, maintaining a percolative path with boundaries $< 5^\circ$ throughout a large region is considered an important criterion for performance. We have used X-ray microbeam diffraction to spatially map the local orientations in a RABiTS sample to investigate how the total angles between neighbouring grains are affected by crystallographic tilting. X-ray Laue patterns were obtained over a 0.73×0.73 mm square area with a step size of $8 \mu\text{m}$. Figure 4 shows colour-coded orientation maps for both the Ni substrate and the oxide buffer generated from the X-ray microbeam Laue measurements. Black lines designate 'blocking' boundaries between adjacent pixels misoriented by a total angle greater than 5° . Each colour indicates a contiguous region connected by paths with misorientations less than 5° . For the Ni substrate, low-angle connectivity extends across the sample in the horizontal, but not the vertical direction. In contrast, enhanced texture in the film due to crystallographic tilts results in larger connected regions and percolation in both the horizontal and vertical directions. The percolation threshold was found to be 5.2° for the substrate and 4.4° for the film in this region.

Although the intergrain misorientations are smaller in the film than in the substrate, the X-ray data show that the intragrain orientation changes (that is, mosaic) increased from $< 0.1^\circ$ within the Ni grains to mosaics of $\sim 0.3^\circ$ in the CeO_2 grains. Thus, the micrometre spatial

resolution of the X-ray microdiffraction technique reveals the existence of subgrain ($< 0.3^\circ$) microstructure in the oxide films. Although the grain size ($\sim 50\text{--}100 \mu\text{m}$) is essentially the same in the film and the substrate, each film grain consists of many small subgrains with slightly different orientations⁵. Consequently, each X-ray diffraction pattern within a particular grain arises from multiple CeO_2 subgrains, with the average orientation typically changing by tenths of a degree over distances of a few micrometres. The superconducting properties will depend on both intergrain and intragrain misorientations. Decreasing a YBaCuO grain boundary from 5.2° to 4.4° typically³⁸ corresponds to a $\sim 25\%$ increase in J_c , and intragrain mosaic may tend to improve the desirable flux-pinning properties of a superconductor³. Thus, the X-ray microdiffraction results demonstrate that understanding and controlling the crystallographic tilts of epitaxial layers can be exploited to enhance transport properties in coated superconductors.

In addition to the lattice orientation, X-ray microbeam Laue diffraction patterns provide a measure of the local deviatoric strain tensor after cooling for each layer^{9,12}. Stress in the oxide layer is of practical importance because it can lead to cracking and delamination^{5,13}. Because dislocations may act to relieve heteroepitaxial stress, it is possible that local strain measurements may reflect the anisotropy associated with the surface miscut ledges, and indirectly reveal dislocation mechanisms in the film. Figure 5a shows the measured diagonal components of the deviatoric strain tensor, ϵ'_{xx} , ϵ'_{yy} and ϵ'_{zz} as a function of the local substrate miscut angle for the CeO_2/Ni sample grown at 600°C . Here z refers to the out-of-plane surface normal direction as shown in Fig. 5b. The deviatoric strain describes the distortion of the shape of the cubic unit cell, and can be combined with the hydrostatic (dilatational) strain to obtain the total strain^{9,12}. Measurements from the Ni substrate showed no strain within the accuracy of these measurements ($\sim 2 \times 10^{-4}$), as would be expected for a ductile, annealed metal substrate.

The CeO_2 measurements reveal biaxial strain in the film at all locations with no dependence on the miscut angle, α . The azimuthal angular dependence of the strain measurements was also examined and no anisotropy was observed. In other words, the local microstrain is approximately equivalent to the macrostrain. Results similar to Fig. 5a

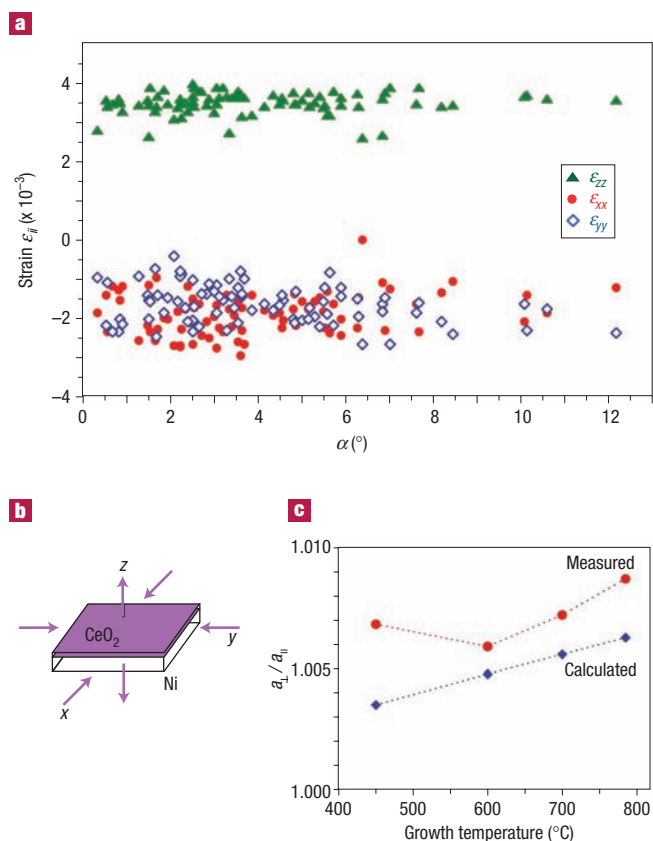


Figure 5 Local strain components in CeO₂ films on textured Ni substrates. **a**, Diagonal components ϵ'_{xx} , ϵ'_{yy} and ϵ'_{zz} of the deviatoric strain tensor for a film grown at 600 °C measured by X-ray microdiffraction. **b**, Biaxial distortion with in-plane compression due to thermal contraction and resulting out-of-plane expansion. **c**, Measured average tetragonality a_{\perp}/a_{\parallel} compared with calculated values due to differential thermal contraction for four different substrate growth temperatures.

were obtained for the samples grown at other substrate temperatures. No dependence of the strain on the local miscut direction or magnitude was found. This result is consistent with the earlier evidence suggesting that strain-relaxation dislocations are not primarily responsible for the crystallographic tilts of the oxide film. Instead, the biaxial strain is due primarily to differential contraction and plume-induced stress³⁹. Figure 5c compares the measured average tetragonality a_{\perp}/a_{\parallel} ratio for the films with values calculated from differential thermal contraction alone. The calculation assumes that a relaxed cubic film is clamped to the substrate at the growth temperature, and that it responds elastically while cooling to room temperature⁴⁰. The excess in the measured compressive strain is attributed to ion damage from the impinging energetic PLD species. This strain is greatest at 450 °C, consistent with the earlier observation that the energetic plume can induce a slight tilt bias at the lowest substrate temperature.

The results reported here illustrate how X-ray microbeam Laue techniques enable new spatially resolved materials investigations, including combinatorial studies. Demonstrating these capabilities, measurements from heteroepitaxial CeO₂ films on textured metal foils reveal growth by ledge propagation at high temperature and by island nucleation at lower temperature. During ledge growth, well-defined, crystallographic tilts of the film relative to the substrate are controlled by the local surface miscut angle as described by a step-matching mechanism. Large-area orientation mapping reveals that the tilts give

rise to enhanced texture and hence greater percolation distances in the oxide film. In practical applications, our results suggest that significant enhancements will be achieved in heteroepitaxial systems with large lattice mismatch, in contrast with conventional growth approaches where lattice mismatch is typically minimized. The tilt mechanisms studied here should be relevant to many oxide/metal systems, including thermal barrier coatings, solar cells, corrosion and interfaces in electronic devices. Thus, the benefits of intentionally enhanced texture should be achievable for many coated materials. Additional experiments examining more localized microstructures such as grain-boundary grooves and crack propagation are now possible with microbeams, and are in progress. Even more broadly, the previously missing ability to obtain spatially resolved structure, orientation and strain information by X-ray microdiffraction will provide unique fundamental information for a wide range of materials disciplines.

Received 3 October 2002; accepted 6 May 2003; published 8 June 2003.

References

- Dimos, D., Chaudhari, P., Mannhart, J. & LeGoues, F. K. Orientation dependence of grain-boundary critical currents in YBa₂Cu₃O_{7- δ} bicrystals. *Phys. Rev. Lett.* **61**, 219–222 (1988).
- Kocks, U. F., Tomé, C. N. & Wenk, H.-R. *Texture and Anisotropy, Preferred Orientations in Polycrystals and their Effect on Materials Properties* (Cambridge Univ. Press, Cambridge, 1998).
- Larbaestier, D., Gurevich, A., Feldmann, D. M. & Polyanski, A. High- T_c superconducting materials for electric power applications. *Nature* **414**, 368–377 (2001).
- Norton, D. P. *et al.* Epitaxial YBa₂Cu₃O₇ on biaxially textured nickel (001): An approach to superconducting tapes with high critical current density. *Science* **274**, 755–757 (1996).
- Norton, D. P. *et al.* Epitaxial YBa₂Cu₃O₇ films on rolled-textured metals for high-temperature superconducting applications. *Mater. Sci. Eng. B* **56**, 86–94 (1998).
- Goyal, A. *et al.* Recent progress in the fabrication of high- J_c tapes by epitaxial deposition of YBCO on RABiTS. *Physica C* **357–360**, 903–913 (2001).
- Ice, G. E. & Larson, B. C. 3D x-ray crystal microscope. *Adv. Eng. Mater.* **2**, 643–646 (2000).
- Tamura, N. *et al.* High spatial resolution orientation and strain mapping in thin films using polychromatic submicron x-ray diffraction. *App. Phys. Lett.* **80**, 3724–3726 (2002).
- Larson, B. C., Yang, W., Ice, G. E., Budai J. D. & Tischler, J. Z. Three-dimensional X-ray structural microscopy with submicrometre resolution. *Nature* **415**, 887–890 (2002).
- Riekel, C. New avenues in x-ray microbeam experiments. *Rep. Prog. Phys.* **63**, 233–262 (2000).
- Poulsen, H. F., Andersen, N. H., Andersen L. G. & Lienert, U., Grain dynamics in Bi-2223 tapes measured by the 3DXRD microscope. *Physica C* **370**, 141–145 (2002).
- Chung, J.-S. & Ice, G. E. Automated indexing for texture and strain measurement with broad-bandpass x-ray microbeams. *J. Appl. Phys.* **86**, 5249–5255 (1999).
- Park, C. *et al.* Bend strain tolerance of critical currents for YBa₂Cu₃O₇ films deposited on rolled-textured (001)Ni. *Appl. Phys. Lett.* **73**, 1904–1906 (1998).
- Nagai, H. Structure of vapor-deposited Ga_{1-x}In_xAs crystals. *J. Appl. Phys.* **45**, 3789–3794 (1974).
- Dodson, B. *et al.* Asymmetric tilt boundaries and generalized heteroepitaxy. *Phys. Rev. Lett.* **61**, 2681–2684 (1988).
- Neumann, D. A., Zabel, H. & Morkoç, H. Terracing in strained-layer superlattices. *J. Appl. Phys.* **64**, 3024–3030 (1988).
- Ayers, J. E., Ghandhi, S. K. & Schowalter, L. J. Crystallographic tilting of heteroepitaxial layers. *J. Cryst. Growth* **113**, 430–440 (1991).
- Aindow, M. & Pond, R. C. On epitaxial misorientations. *Phil. Mag.* **A63**, 667–694 (1991).
- Riesz, F. Crystallographic tilting in lattice-mismatched heteroepitaxy: A Dodson-Tsao relaxation approach. *J. Appl. Phys.* **79**, 4111–4117 (1996).
- Theis, C. D. & Schlom D. G. Domain structure of epitaxial PbTiO₃ films grown on vicinal SrTiO₃. *J. Mater. Res.* **12**, 1297–1305 (1997).
- Jain, S. C., Harker, A. H. & Cowley, R. A. Misfit strain and misfit dislocations in lattice mismatched epitaxial layers and other systems. *Phil. Mag.* **A75**, 1461–1515 (1997).
- Pashley, D. W. Epitaxy growth mechanisms. *Mater. Sci. Technol.* **15**, 2–8 (1999).
- Pesek, A., Hinger, K., Riesz, F. & Lischka, K. Lattice misfit and relative tilt of lattice planes in semiconductor heterostructures. *Semicond. Sci. Technol.* **6**, 705–708 (1991).
- Ressler, K. G., Sonnenberg, N. & Cima, M. J. Mechanism of biaxial alignment of oxide thin films during ion-beam assisted deposition. *J. Am. Ceram. Soc.* **80**, 2637–2648 (1997).
- Bauer, M., Semerad R. & Kinder, H. YBCO films on metal substrates with biaxially aligned MgO buffer layers. *IEEE Trans. Appl. Supercon.* **9**, 1502–1505 (1999).
- Ernst, F. Metal-oxide interfaces. *Mat. Sci. Eng. R* **14**, 97–156 (1995).
- Cantoni, C. *et al.* Reflection high-energy electron diffraction studies of epitaxial oxide seed-layer growth on rolling-assisted biaxially textured substrate Ni(001): The role of surface structure and chemistry. *App. Phys. Lett.* **79**, 3077–3079 (2001).
- Sun, E. Y. *et al.* High-resolution TEM/analytical electron microscopy characterization of epitaxial oxide multilayers fabricated by laser ablation on biaxially textured Ni. *Physica C* **321**, 29–38 (1999).
- Park, C. *et al.* Nucleation of epitaxial yttria-stabilized zirconia on biaxially textured (001) Ni for deposited conductors. *App. Phys. Lett.* **76**, 2427–2429 (2000).
- Aytug, T. *et al.* La_{2-x}STr_xMnO₇: A single, conductive-oxide buffer layer for the development of YBa₂Cu₃O_{7- δ} coated conductors. *App. Phys. Lett.* **79**, 2205–2207 (2001).
- Hilgenkamp, H. & Mannhart, J. Grain boundaries in high- T_c superconductors. *Rev. Mod. Phys.* **74**, 485–549 (2002).
- Rhyner, J. & Blatter, G. Limiting-path model of the critical current in a textured YBa₂Cu₃O_{7- δ} film. *Phys. Rev. B* **40**, 829–832 (1989).
- Specht, E. D., Goyal, A. & Kroeger, D. M. Scaling of percolative current flow to long lengths in biaxially textured conductors. *Supercond. Sci. Technol.* **13**, 592–597 (2000).

34. Rutter, N. A., Glowacki, B. A. & Evetts, J. E. Percolation modelling for highly aligned polycrystalline superconducting tapes. *Supercond. Sci. Technol.* **13**, L25–L30 (2000).
35. Feldmann, D. M. *et al.* Influence of nickel substrate grain structure on $\text{YBa}_2\text{Cu}_3\text{O}_{7-x}$ supercurrent connectivity in deformation-textured coated conductors. *Appl. Phys. Lett.* **77**, 2906–2908 (2000).
36. Holzapfel, B. *et al.* Grain boundary networks in Y123 coated conductors: formation, properties and simulation. *IEEE Trans. Appl. Supercon.* **11**, 3872–3875 (2001).
37. Nakamura, Y., Izumi, T. & Shiohara, Y. Percolation analysis of the effect of tape length on the current density of 123 coated conductors. *Physica C* **371**, 275–284 (2002).
38. Verebelyi, D. T. *et al.* Low angle grain boundary transport in $\text{YBa}_2\text{Cu}_3\text{O}_{7-\delta}$ coated conductors. *Appl. Phys. Lett.* **76**, 1755–1757 (2000).
39. Norton, D. P., Park, C., Budai, J. D., Pennycook, S. J. & Proureau, C. Plume-induced stress in pulsed-laser deposited CeO_2 films. *Appl. Phys. Lett.* **74**, 2134–2136 (1999).
40. Hornstra, J. & Bartels, W. J. Determination of the lattice constant of epitaxial layers of III-V compounds. *J. Cryst. Growth* **44**, 513–517 (1978).

Acknowledgements

We thank K.-S. Chung, E. Williams, and W. P. Lowe for their contributions during this work, 3M Company for supplying the Ni substrates, and T. Aytug for providing the LMO samples. The measurements were performed on the UNI-CAT and MHATT-CAT beam lines at the Advanced Photon Source (APS) at Argonne National Laboratory, which is supported by the US Department of Energy, Office of Science. This research was sponsored by the US Department of Energy Basic Energy Sciences, Division of Materials Sciences, under contract with Oak Ridge National Laboratory, managed by UT-Battelle, LLC.

Correspondence and requests for materials should be addressed to J.D.B.

Competing financial interests

The authors declare that they have no competing financial interests.